Journal of Sound and Vibration (2001) **244**(4), 669–684
doi:10.1006/jsvi.2000.3488, available online at http://www.idealibrary.com on IDEAL®

PRIMARY AND PARAMETRIC NON-LINEAR RESONANCES OF A POWER TRANSMISSION BELT: EXPERIMENTAL AND THEORETICAL ANALYSIS

F. Pellicano

Dipartimento di Scienze dell'Ingegneria, Università di Modena e Reggio Emilia, via Vignolese 905, *I*-41100 *Modena, Italy. E-mail: frank@unimo.it*

A. Fregolent and A. Bertuzzi

Dipartimento di Meccanica e Aeronautica, Università di Roma "La Sapienza", via Eudossiana 18, *I*-00184 *Rome, Italy*

and

F. Vestroni

Dipartimento di Ingegneria Strutturale e Geotecnica, Università di Roma "La Sapienza", via Eudossiana 18, *I*-00184 *Rome, Italy*

(*Received* 9 *May* 2000, *and in final form* 2 *November* 2000)

In this paper, the effect of pulley eccentricity on the vibration of a power transmission belt is experimentally investigated and a theoretical model is developed for validation and identification purposes. This eccentricity gives rise to dangerous operating conditions for the system, especially when it excites the frequency range of the belt resonances. As expected, the system shows a hardening non-linear behavior. Moreover, the fluctuation of the belt tension, due to the pulley eccentricity, gives rise to a parametric instability that can cause catastrophic failures of the structure. Laser displacement transducers are used to measure transversal vibrations of the belt. An approximate analytical solution of the travelling beam dynamics is developed in order to model the system and reproduce the experimental data. Comparisons between analytical solution and experimental data allow the identification of the unknown parameters of the analytical model. A validation of the identified model is performed by comparing analytical and experimental data in different operating conditions.

1. INTRODUCTION

In many mechanical applications, power transmission belts play a fundamental role: power transmission between axes, high-precision motion transmission, synchronization of movements and so on, represent some examples of applications. Moreover, the physical and mathematical model describing the dynamics of a power transmission belt is suitable to model several mechanical systems such as high-speed magnetic tapes, band saw blades, aerial cable threadlines, and sheet production processes. All previous systems belong to the class of axially moving systems.

The dynamic behavior of an axially moving system is greatly influenced by the presence of the transport of mass. When a critical value of the axial speed is reached, the first linear

0022-460X/01/290669 + 16 $35.00/0

natural frequency vanishes; the straight equilibrium position loses stability and bifurcates into new equilibrium states. In the sub-critical speed range, all natural frequencies decrease as the axial speed increases and the vibration modes are complex, even if the system is conservative.

In actual operating conditions, power transmission belts are subjected to many external disturbances, such as pulley eccentricity, irregularities of the belt surface and non-stationary driving motor rotation speed. When an oscillating external excitation causes a resonance, very dangerous conditions may be found and the axially moving continuum may produce catastrophic failures, as in the case of parametric instability.

Analytical models for axially moving systems have been extensively studied in the last 50 years. Ashley and Haviland [1], Swope and Ames [2], Mote [3], Thurman and Mote [4] were the pioneers in this research area. Recently, in reference [5], the study of the problem of axially moving beams has been tackled in a more systematic way. In reference [6] the non-linear vibrations and bifurcations of moving beams were investigated in sub- and super-critical speed ranges, and a local analysis for non-linear oscillations was performed.

Many other papers have been devoted to the analysis of the dynamic behavior of these systems. A literature overview can be found in reference [7]. Some of these papers deal with aspects close to the subject of the present work. Ulsoy *et al.* [8] studied instability phenomena of a belt tensioner system, including linear parametric instability, and made qualitative comparisons between numerical and experimental data. Mockensturm *et al.* [9] studied analytically the effect of a tension fluctuation, giving stability bounds of stationary solutions. Hwang *et al.* [10] developed a non-linear model to describe the longitudinal response of automotive serpentine belts and to predict the belt slip due to the dynamic tension fluctuation. Moon and Wickert [11] studied experimentally the dynamic behavior of a power transmission tooth belt in the presence of two in-phase pulley eccentricities, validating the analytical model proposed in reference [6]. They used a Laser Doppler vibrometer to measure transversal vibrations of the moving rubber surface. The experimental results confirmed the hardening character of the non-linearity. Similar results were obtained in reference [12], where a Laser Doppler vibrometer was used to measure vibrations of a flat belt with a single eccentric pulley.

In the present work, an experimental and theoretical study of the non-linear vibrations of a power transmission belt is performed. Large vibration amplitudes due to several resonance conditions are experimentally observed and analytically justified. A Laser Telemeter is used to measure the response of the moving belt. Only the driven pulley presents an eccentricity, which produces two different excitations: seismic and parametric. The amplitude frequency curve is experimentally obtained in the case of primary resonance, due to seismic excitation. The experimental curve is fitted with that of an analytical model, which is obtained in an approximate closed form. The fitting allows for the setting of some unknown parameters of the analytical model. The identified model is used to simulate the belt vibrations in parametric resonance and the results of the simulations are compared with the experimental data.

2. ANALYTICAL MODEL

In this section, an analytical model is presented for the transversal vibrations of an axially moving one-dimensional continuum. First of all, a simply supported Euler–Bernoulli beam model is considered, with the inclusion of the effects of body forces due to the axial transport of mass and the geometric effect due to stretching of the beam axis (Figure 1). Then, flexural stiffness is neglected and the simpler axially moving string equation is analyzed. This model

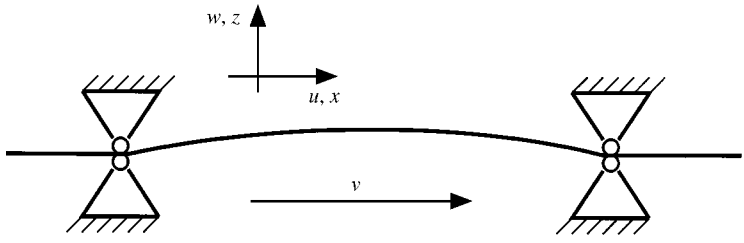

Figure 1. Model of the travelling beam.

does not include boundary effects due to the pulley curvature and multi-span interactions, studied in references [13–17]. However, its effectiveness in explaining the experimental results together with its simplicity makes it very useful. The same model was already adopted in the literature [11] to study the effect of seismic excitation caused by two in-phase eccentric pulleys.

When an eccentricity of one pulley only is present, as in many actual problems, the seismic excitation is associated with a tension fluctuation, and the excitation frequency is equal to the angular velocity of the pulley. The dynamics of the system can be described by an integro-differential equation, which involves the transverse displacement $w(x, t)$ only, after static condensation of the longitudinal strain [4–7]:

$$v_f^2 \frac{\partial^4 w}{\partial x^4} + (v^2 - 1 + p(t)) \frac{\partial^2 w}{\partial x^2} + 2v \frac{\partial^2 w}{\partial x \partial t} + \frac{\partial^2 w}{\partial t^2} = \frac{v_T^2}{2} \frac{\partial^2 w}{\partial x^2} \int_0^1 \left(\frac{\partial w}{\partial \sigma} \right)^2 \mathrm{d}\sigma \tag{1a}$$

with the following boundary conditions:

$$w(0, t) = w_0(t), \quad w(1, t) = 0 \tag{1b}$$

$$\frac{\partial^2 w}{\partial x^2}(0, t) = \frac{\partial^2 w}{\partial x^2}(1, t) = 0 \tag{1c}$$

Suitable initial conditions complete the Cauchy problem.

The following non-dimensional terms describe equations (1a–c) from the physical point of view: $w = \tilde{w}/\ell$, $x = \tilde{x}/\ell$, $t = \tilde{t}\sqrt{P/\rho A \ell^2}$, $v = \tilde{v}/\sqrt{P/\rho A}$, $v_T = \sqrt{EA/P}$, $v_f = \sqrt{EI/P\ell^2}$, $p(t) = \tilde{p}(t)/P$; where ℓ is the beam length, $\tilde{x}$ the axial co-ordinate, $\tilde{w}$ the transversal displacement field, $\tilde{t}$ the time, $\tilde{v}$ the axial speed, P the initial tension, $\tilde{p}$ the tension fluctuation, $\tilde{w}_0 = \ell w_0$ the seismic excitation, ρ the mass density, A the cross section area, E the Young modulus, I the area moment. The terms $2v\partial^2 w/\partial x \partial t$ and $v^2 \partial^2 w/\partial x^2$ represent the Coriolis and centrifugal forces respectively, whereas the remaining terms are well known in the beam-string theory and do not require explanation.

The linear operator is skew symmetric due to the presence of Coriolis forces, which imply complex vibration modes, even though no damping is included in the model and the system is Hamiltonian. The centrifugal forces cause a decrease in the natural vibration frequencies, and at a critical value of the axial speed $v_{cr} = \sqrt{1 + \pi^2 v_f^2}$, they cause a loss of stability and static bifurcation.

In order to analyze the seismic excitation it is useful to introduce a new variable, which eliminates the rigid body motion due to the support displacement:

$$w(x, t) = \hat{w}(x, t) + (1 - x) w_0(t).$$

Equation (1a) becomes

$$v_f^2 \frac{\partial^4 \hat{w}}{\partial x^4} + (v^2 - 1 + p(t)) \frac{\partial^2 \hat{w}}{\partial x^2} + 2v \frac{\partial^2 \hat{w}}{\partial x \partial t} + \frac{\partial^2 \hat{w}}{\partial t^2} - 2v \frac{\partial w_0}{\partial t} + \frac{\partial^2 w_0}{\partial t^2}(1 - x)$$

$$= \frac{v_T^2}{2} \frac{\partial^2 \hat{w}}{\partial x^2} \left(\int_0^1 \left(\frac{\partial \hat{w}}{\partial \sigma} \right)^2 \mathrm{d}\sigma + w_0^2 \right) \tag{2}$$

Usually, w_0 is very small, then the term $(v_T^2/2)(\partial^2 \hat{w}/\partial x^2)(w_0^2)$ can be neglected. The boundary conditions (1b, c) become

$$\hat{w}(0, t) = 0, \quad \hat{w}(1, t) = 0, \tag{3}$$

$$\frac{\partial^2 \hat{w}}{\partial x^2}(0, t) = \frac{\partial^2 \hat{w}}{\partial x^2}(1, t) = 0. \tag{4}$$

Equation (2) illuminates two interesting aspects of the problem of a belt running on a series of pulleys, in which at least one of them presents an eccentricity: (1) *a direct excitation* due to the inertial terms $\partial^2 w_0/\partial t^2 - 2v\partial w_0/\partial t$; (2) a *parametric excitation* $p(t)$ due to tension fluctuation. It is to be noted that both $p(t)$ and $w_0(t)$ are harmonic and their frequency is $\omega = \tilde{v}/R$ rad/s, where R is the pulley radius.

When the beam length is large with respect to the thickness, the flexural stiffness is negligible and the first term in equation (2) can be omitted. In this case, the eigenfunctions of the linearized system are known analytically [5], and can be used to expand the solution. In the following, a single mode expansion will be used to apply the Galerkin procedure to the non-linear problem. Even though a single mode expansion is a great simplification, it permits the finding of a perturbative approximation of the solution through simple analytical formulas. For the purposes of the present work, such formulas can be sufficient to explain and justify the experimental evidence and to identify the main system parameters.

2.1. SINGLE MODE EXPANSION AND GALERKIN PROJECTION

In order to study analytically problem (2) and (3) with the simplifications outlined in the previous section, i.e., neglecting the flexural stiffness and the related terms in equations (2) and (4), it is useful to introduce the following operators:

$$\mathbf{A} = \begin{bmatrix} I & 0 \\ 0 & (v^2 - 1)\dfrac{\partial^2}{\partial x^2} \end{bmatrix}, \quad \mathbf{B} = \begin{bmatrix} 2v\dfrac{\partial}{\partial x} & (v^2 - 1)\dfrac{\partial^2}{\partial x^2} \\ -(v^2 - 1)\dfrac{\partial^2}{\partial x^2} & 0 \end{bmatrix}, \quad \mathbf{C} = \begin{bmatrix} 0 & \dfrac{\partial^2}{\partial x^2} \\ 0 & 0 \end{bmatrix},$$

and the following vectors:

$$\hat{\hat{\mathbf{w}}} = [\hat{\hat{w}}, \hat{w}]^{\mathrm{T}}, \quad \mathbf{F}(\hat{\mathbf{w}}, t) = \left[\left(2v\dot{w}_0 - \ddot{w}_0(1 - x) + \frac{v_T^2}{2} \frac{\partial^2 \hat{w}}{\partial x^2} \int_0^1 \left\{ \frac{\partial \hat{w}}{\partial x} \right\}^2 \mathrm{d}x \right), \quad 0 \right]^{\mathrm{T}};$$

where $\dot{w} \equiv \partial w/\partial t$ and $\ddot{w} \equiv \partial^2 w/\partial t^2$.

Equation (2) becomes

$$\mathbf{A}\hat{\hat{\mathbf{w}}} + \mathbf{B}\hat{\mathbf{w}} + p(t)\mathbf{C}\hat{\mathbf{w}} = \mathbf{F}(\hat{\mathbf{w}}, t) \tag{5}$$

Without external excitations, the eigenvalue problem associated with the linearized equation (5) is

$$\lambda \mathbf{A}\boldsymbol{\phi} + \mathbf{B}\boldsymbol{\phi} = 0, \tag{6}$$

where λ is an eigenvalue and the vector $\boldsymbol{\phi}(x)$ is an eigenfunction, which presents the following structure: $\boldsymbol{\phi}(x) = [\lambda\psi(x), \psi(x)]^{\mathrm{T}}$, where $\psi(x)$ is a complex function. The solution of the eigenproblem (6), with the boundary conditions (3), furnishes infinite eigenvalues and eigenfunctions, which were analytically evaluated in reference [5]: $\lambda_n = \mathrm{j}\omega_n = \mathrm{j}n\pi(1 - v^2)$, $\psi_n = d_n \exp(\mathrm{j}n\pi v x) \times \sin n\pi x$, $n = \pm 1, \ \pm 2, \ldots$; where $\mathrm{j} = \sqrt{-1}$ and d_n is an arbitrary constant assumed to be equal to $1/n$ in the following.

The following metric is introduced to perform projections: $\langle \mathbf{f}_1(x), \mathbf{f}_2(x) \rangle = \int_0^1 \mathbf{f}_1^{\mathrm{T}}(x)\mathbf{f}_2^*(x)\,\mathrm{d}x$, where the symbol "*" indicates the complex conjugate. Using the previously mentioned formalism, the following orthogonality properties of the eigenfunctions can be found:

$$\langle \mathbf{A}\boldsymbol{\phi}_n, \boldsymbol{\phi}_m \rangle = M_n \delta_{nm}, \qquad \langle \mathbf{B}\boldsymbol{\phi}_n, \boldsymbol{\phi}_m \rangle = M_n \lambda_n \delta_{nm}, \quad n = \pm 1, \ \pm 2, \ldots, \tag{7}$$

where δ_{nm} is the Kronecker symbol, $\boldsymbol{\phi}_{-n} = \boldsymbol{\phi}_n^*$ and $\lambda_{-n} = \lambda_n^*$. For a single complex mode expansion, such properties suggest the following expression of $\hat{\mathbf{w}}$:

$$\hat{\mathbf{w}}(x, t) = \xi_n(t)\boldsymbol{\phi}_n(x) + \xi_n^*(t)\boldsymbol{\phi}_n^*(x) \tag{8}$$

The Galerkin procedure gives

$$\begin{aligned} M_n \dot{\xi}_n - M_n \lambda_n \xi_n + p(t)\langle \mathbf{C}(\xi_n(t)\boldsymbol{\phi}_n(x) + \xi_n^*(t)\boldsymbol{\phi}_n^*(x)), \boldsymbol{\phi}_n(x) \rangle \\ = \langle \mathbf{F}[(\xi_n(t)\boldsymbol{\phi}_n(x) + \xi_n^*(t)\boldsymbol{\phi}_n^*(x)), t], \boldsymbol{\phi}_n(x) \rangle \end{aligned} \tag{9}$$

The complex conjugate of equation (9) must be formally included in the analysis. Moreover, for the purposes of the present work, $n = 1$ is the case of interest. In fact, experimental data regard primary and subharmonic parametric resonances of the first mode.

As the imposed support displacement $w_0(t)$ is small, a suitable ordering is introduced: $w_0(t) = \varepsilon^3 \bar{W}_0 \cos \Omega t$, $p(t) = \varepsilon\bar{p}(t) = \varepsilon\bar{p}_1 \cos \Omega t$ and $\xi_1 = \varepsilon\bar{\xi}_1$, and $\Omega = \omega/\sqrt{P/(\rho A l^2)}$. Moreover, a modal damping $\mu_1 = 2\delta_1\omega_1 = \varepsilon^2\tilde{\mu}_1$ is introduced. For the sake of simplicity, the symbol "bar" is dropped and the modal equation (9) can be rewritten as

$$\begin{aligned} \dot{\xi}_1 = \lambda_1 \xi_1 + \varepsilon p_1(t)(c_1 \xi_1 + c_2 \xi_1^*) + \varepsilon^2 \mu_1 \xi_1 \\ + \varepsilon^2 (A_1 \xi_1^3 + A_2 \xi_1^2 \xi_1^* + A_3 \xi_1 \xi_1^{*2} + A_4 \xi_1^{*3} - \Omega^2 A_5 W_0 \cos \Omega t + \mathrm{j}\Omega A_6 W_0 \sin \Omega t), \end{aligned} \tag{10}$$

where the coefficients are defined in Appendix A.

The set of complex ordinary differential equations given by equation (10) and its complex conjugate is now analyzed through the method of normal forms [18–20]. The method is based upon a non-linear change of co-ordinates whose goal is to eliminate the non-linear part of the system as much as possible. The simplified form of the system is called the normal form, which is linear only when the system is hyperbolic, according to the Hartmann Grobmann theorem [21].

Two different cases are considered here: (1) *primary resonance*, $\Omega \cong \omega_1$; (2) *parametric resonance*, $\Omega \cong 2\omega_1$. In case (1) equation (10) is studied neglecting the parametric excitation

that is not resonant, i.e., $p(t) = 0$; in case (2) all terms are retained even though, in the normal form, the direct excitation disappears.

2.2. PRIMARY RESONANCE

The method of normal forms can be applied to autonomous systems only. In order to apply this method, the non-autonomous system (10) is transformed into an autonomous one by introducing a new variable:

$$\dot{\xi}_2 = \mathrm{j}\Omega\xi_2 \Rightarrow \xi_2 = \frac{\exp(\mathrm{j}\Omega t)}{2} \tag{11}$$

so that the external excitation can be rewritten as $W_0(-\Omega^2 A_5(\xi_2 + \xi_2^*) + \mathrm{j}\Omega A_6(\xi_2 - \xi_2^*))$. If the excitation frequency is close to the first linear natural frequency, one can introduce an ordering parameter: $\varepsilon^2\sigma = \omega_1 - \Omega$.

The non-linear change of variables is

$$\xi_i = \eta_i + \varepsilon^2 h_i(\eta_1, \eta_2, \eta_1^*, \eta_2^*) + O(\varepsilon^3), \quad i = 1, 2, \tag{12}$$

where the functions h_i present the same structure of the non-linear portion of dynamical system to be cancelled. Accurate details of the procedure used here can be found in reference [22].

The transformation (12) leads to the normal form

$$\dot{\eta}_1 = \mathrm{j}\Omega\eta_1 + \mathrm{j}\varepsilon^2\sigma\eta_1 + \varepsilon^2\frac{\mu_1}{2}\eta_1 + \varepsilon^2 A_2\eta_1^2\eta_1^* + \varepsilon^2 q\exp(\mathrm{j}\Omega t), \tag{13}$$

where $q = W_0(-\Omega^2 A_5 + \mathrm{j}\Omega A_6)/2$. It must be pointed out that A_5 and A_6 are complex quantities, so that the coefficient q can be rewritten as $q = q_R + \mathrm{j}q_I$. A_2 is imaginary, according to the definition given in Appendix A.

A further transformation $\eta_1(t) = \zeta_1(t)\exp(\mathrm{j}\Omega t)$ is useful to solve equation (13); such "demodulation" allows filtering out fast oscillations and studying the steady oscillatory states as fixed points of the following dynamical system:

$$\dot{\zeta}_1 = \mathrm{j}\varepsilon^2\sigma\zeta_1 + \varepsilon^2\frac{\mu_1}{2}\zeta_1 + \varepsilon^2 A_2\zeta_1^2\zeta_1^* + \varepsilon^2 q. \tag{14}$$

Fixed points of equation (14) and its complex conjugate can be easily found by using Cartesian co-ordinates, i.e., by separating real and imaginary parts, by letting: $\zeta_1 = a + \mathrm{j}b$, $A_2 = \mathrm{j}d$:

$$\frac{\mu_1 a}{2b} + a^2 d + b^2 d + \frac{q_R}{b} - \sigma = 0, \tag{15a}$$

$$\frac{\mu_1 b}{2a} + a^2 d + b^2 d + \frac{q_I}{a} + \sigma = 0. \tag{15b}$$

By summing equation (15a) with equation (15b) σ can be eliminated and the solution $a = a(b)$ or $b = b(a)$ can be easily found. Only the real solutions are retained and substituted into equation (15a) or (15b), then the parameter σ corresponding to the given amplitude of

oscillation is obtained. The actual response of the system is

$$\hat{\mathbf{w}}(x,t) = \varepsilon(a + \mathrm{j}b)\boldsymbol{\phi}_1(x)\exp(\mathrm{j}\Omega t) + \varepsilon(a - \mathrm{j}b)\boldsymbol{\phi}_1^*(x)\exp(-\mathrm{j}\Omega t) + O(\varepsilon^2), \tag{16}$$

i.e., the transverse displacement is given by

$$\hat{w}(x,t) = \varepsilon(a + \mathrm{j}b)\psi_1(x)\exp(\mathrm{j}\Omega t) + \varepsilon(a - \mathrm{j}b)\psi_1^*(x)\exp(-\mathrm{j}\Omega t) + O(\varepsilon^2), \tag{17}$$

where the ordering parameter ε can be included in the amplitude $a + \mathrm{j}b$.

The previous expression furnishes the amplitude frequency response curve, which will be compared to the experimental curve. The parameter settings in equations (15a, b) deserve special care: both the damping ratio δ_1 and the non-linear parameter v_T, which affect coefficients μ_1 and d, cannot be easily estimated, so that they are evaluated by comparing experimental and theoretical responses. In the present s.d.o.f. system, the parameter identification is quite simple, since only two parameters must be identified. Therefore, no optimization algorithms are developed, and the identification is obtained by simply adapting the theoretical response to measured data.

2.3. PARAMETRIC RESONANCE

After introducing the new variable $\dot{\xi}_2 = \mathrm{j}\Omega\xi_2$, the term $p(t)$, due to the tension fluctuation, can be rewritten as $p(t) = \varepsilon p_1(\xi_2 + \xi_2^*)/2$. The variable ξ_2 transforms a parametrically excited system with cubic non-linearities into an equivalent autonomous system with quadratic and cubic non-linearities. When the excitation frequency is almost two times the first linear natural frequency, an ordering parameter can be introduced: $\varepsilon^2\sigma = 2\omega_1 - \Omega$.

The following non-linear change of variables is used:

$$\xi_i = \eta_i + \varepsilon h_{1,i}(\eta_1, \eta_2, \eta_1^*, \eta_2^*) + \varepsilon^2 h_{2,i}(\eta_1, \eta_2, \eta_1^*, \eta_2^*) + O(\varepsilon^3), \quad i = 1, 2, \tag{18}$$

where the functions $h_{j,i}$ present the same structure of the portion of the dynamical system that is to be eliminated. The normal form of the system is

$$\dot{\eta}_1 = \mathrm{j}\frac{\Omega}{2}\eta_1 + \varepsilon c_2 p_1 \eta_2 \eta_2^* + \mathrm{j}\varepsilon^2\sigma\eta_1 + \varepsilon^2\frac{\mu_1}{2}\eta_1 + \varepsilon^2 A_2 \eta_1^2\eta_1^* - \mathrm{j}\varepsilon^2\frac{c_2 c_2^*}{2\Omega}p_1^2\eta_1\eta_2\eta_2^*, \tag{19}$$

where $\eta_2 \equiv \xi_2$. Taking into account the definition of ξ_2 and introducing the slow variable ζ_1, one has $\eta_1 = \zeta_1\exp(\mathrm{j}\Omega t/2)$. This transformation gives

$$\dot{\zeta}_1 = \mathrm{j}\varepsilon^2\sigma\zeta_1 + \varepsilon\frac{c_2}{2}p_1\zeta_1^* + \varepsilon^2\frac{\mu_1}{2}\zeta_1 + \varepsilon^2 A_2\zeta_1^2\zeta_1^* - \mathrm{j}\varepsilon^2\frac{|c_2^2|}{8\Omega}p_1^2\zeta_1. \tag{20}$$

Recalling that $c_2 = c_2^R + \mathrm{j}c_2^I$ is complex, and introducing Cartesian co-ordinates, the fixed points of equation (20) can be studied by separating real and imaginary parts and putting to zero the time derivatives:

$$\varepsilon\frac{\mu_1 a}{2} + \frac{c_2^R p_1}{2}a + \frac{c_2^I p_1}{2}b + \varepsilon\frac{(c_2^{R^2} + c_2^{I^2})p_1^2}{8\Omega}b - \varepsilon a^2 bd - \varepsilon b^3 d - \varepsilon\sigma b = 0, \tag{21a}$$

$$\varepsilon\frac{\mu_1 b}{2} - \frac{c_2^R p_1}{2}b + \frac{c_2^I p_1}{2}a - \varepsilon\frac{(c_2^{R^2} + c_2^{I^2})p_1^2}{8\Omega}a + \varepsilon ab^2 d + \varepsilon a^3 d + \varepsilon\sigma a = 0. \tag{21b}$$

By following the procedure outlined in the previous section and using the values of parameters identified in the primary resonance, the amplitude frequency diagrams are obtained and compared with the experimental data.

3. EXPERIMENTAL SET-UP AND RESULTS

The experiments deal with a power transmission belt, Figure 2. A flat rubber belt with joint runs on two pulleys, whose diameter is 0·2 m and the distance between axes is 1·01 m. A fixed tensioner is present on the lower branch. The driven pulley (on the left in Figure 2) has variable eccentricity, whereas the driver pulley does not present eccentricity. The aim of the tests is the measurement of the vibration amplitude when both axial speed and pulley eccentricity are varied.

A laser telemeter is used to measure directly the transverse displacement of the belt. The axial motion of the belt surface does not pollute measurements obtained with this device. The telemeter cut-off frequency is 1000 Hz, and is sufficient in the specific experiments; in fact, the natural frequencies of the lower modes are in the order of some tens of Hz. In resonance conditions, a large eccentricity can cause an amplitude of oscillation in the order of 0·2 m in the middle of the upper belt span. The telemeter range is 0·04 m; therefore, the transducer is located in proximity of the right pulley, where the amplitude of oscillation is within measurement limits. The closeness of the constraint does not greatly affect the measurement; indeed, a good agreement is found between theoretical forecasts of the identified model and experimental data.

3.1. PRIMARY RESONANCE

A first series of tests deal with the behavior of the system in primary resonance conditions with different pulley eccentricities. In this situation, the external excitation frequency $\omega = \tilde{v}/R$ is close to the first natural frequency of the system, which is; $\tilde{\omega}_1 = (\pi/l)\sqrt{(\rho A/P)}((p/\rho A) - \tilde{v}^2)$ rad/s. In Figure 3, a qualitative comparison between the successive configurations of the belt during an undamped free oscillation, originated by an initial condition coincident with the first analytical mode [Figure 3(a)], and the actual vibration shape in resonance condition [Figure 3(b)] is shown. The second picture is obtained by illuminating the vibrating belt with a stroboscopic lamp. It is interesting to note that the first mode is mainly given by a summation of the fundamental shape $\sin \pi x$, which represents the linear mode at $v = 0$, and the second wave $\sin 2\pi x$. This feature, predicted from theoretical models [7], is in good agreement with the experimental evidence.

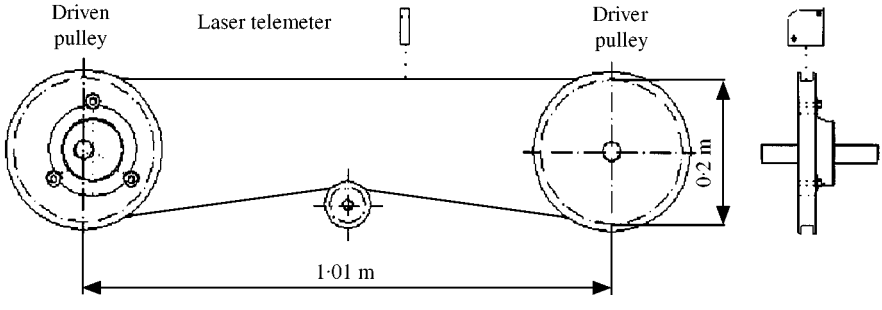

Figure 2. Experimental set-up.

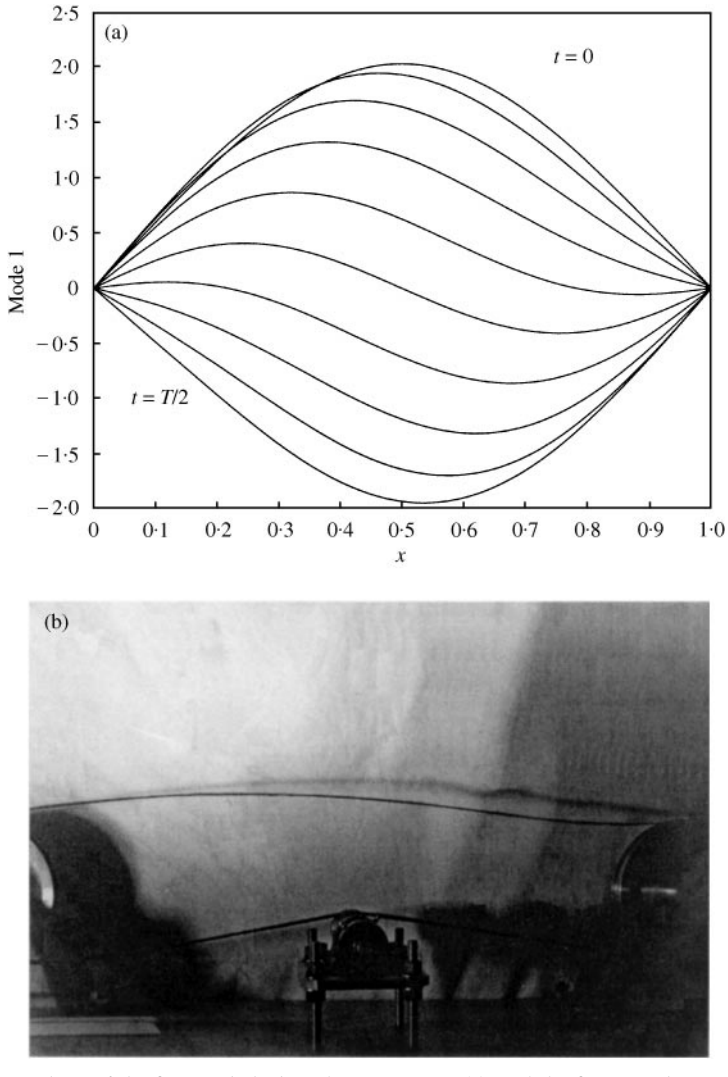

Figure 3. Snapshots of the first analytical mode at $= 95\% v_{cr}$ (a), and the first experimental mode (b).

In Figure 4(a) a quantitative experimental result is presented for the following eccentricity: $\tilde{w}_0 = 0{\cdot}004$ m. The behavior of the stationary amplitude of vibration in correspondence with the measurement point versus the excitation frequency, in the neighborhood of the first linear natural frequency, is shown. Dots represent the actual amplitudes; balls represent the average values. The excitation level $w_0 = \tilde{w}_0/L$ is known and the measurement of the linear natural frequency at $v = 0$, $\tilde{\omega}_{1,v=0} = 2\pi 24{\cdot}5$ rad/s, allows one to estimate the value of the resonance frequency, which is $\tilde{\omega}_{1,v\neq 0} = 2\pi 22{\cdot}5$ rad/s. Suitable values of damping ratio and non-linear parameter, $v_T = 6$ and $\delta_1 = 0{\cdot}026$, are found by adapting the theoretical response obtained through the perturbation approach reported in the previous section to the experimental data. No special algorithms are used to this end. These values are used to draw the analytical backbone and amplitude–frequency curves, continuous lines, in Figure 4(a).

A second series of measurements is performed with a slightly different belt pre-tension with respect to the previous case. The following eccentricities are considered: $\tilde{w}_0 = 0{\cdot}0032$,

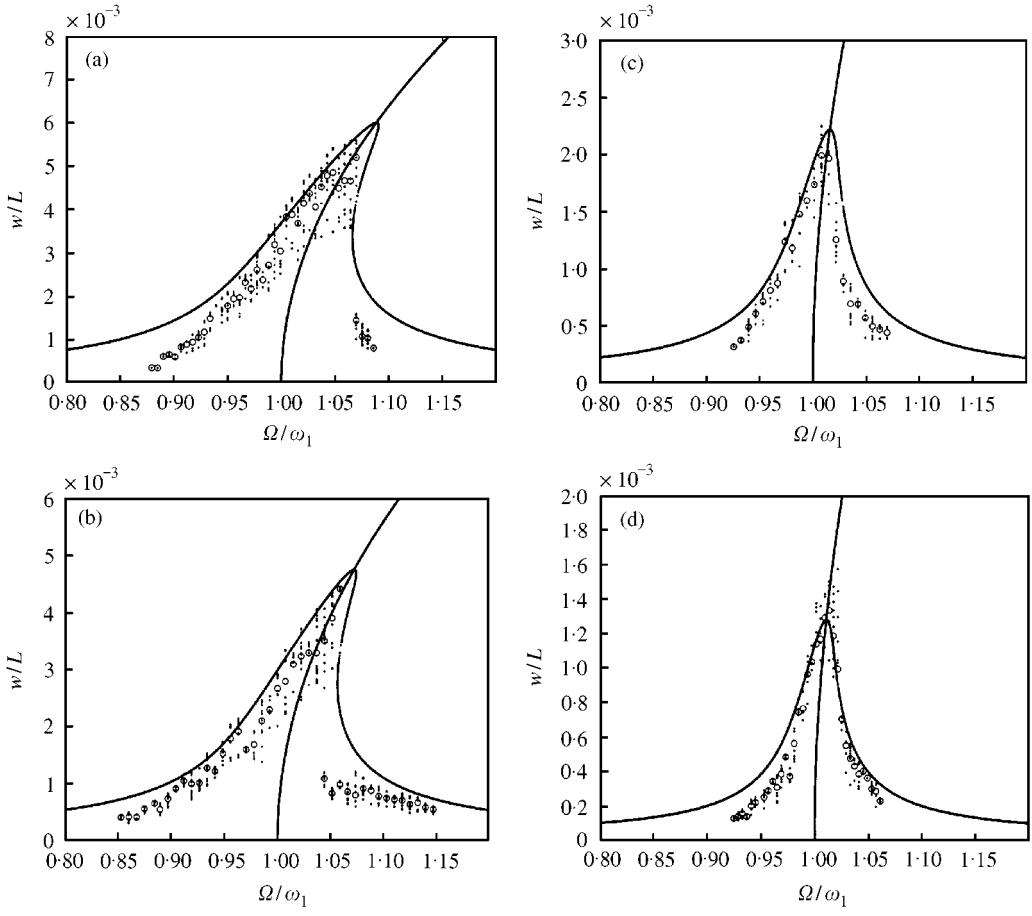

Figure 4. Frequency amplitude curves. Primary resonance, eccentricity: (a) 0·004 m; (b) 0·0032 m; (c) 0·0013 m; (d) 0·0006 m; (·) measured amplitude; (○) mean amplitude; (——) analytical solution.

0·0013 and 0·0006 m; the experimental results, compared with the analytical fitting curves, are presented in Figures 4(b–d). In Table 1 the main parameters used to obtain the best fitting are listed (note that also the case $\tilde{w}_0 = 0{\cdot}004$ m with different tension is included). The different magnitude of $\omega_{1,v=0}$ is due to the different tension and also due to the variable operating temperature of the belt, which increases with the eccentricity, i.e., with the belt stress. The damping ratio has been found to be almost constant; conversely, the non-linear parameter v_T is significantly different for the case $\tilde{w}_0 = 0{\cdot}0006$ m. This discrepancy can be easily explained: for a very small amplitude of vibration, the system response is almost linear and the identification of the correct backbone is affected by large errors.

The asymmetry and folding due to the presence of a hardening non-linearity are observable. Note that the experimental data do not match the peak of the analytical curves. This is clearer for the case $\tilde{w}_0 = 0{\cdot}004$ and 0·0032 m. Indeed, the basin of attraction of the upper stable branch becomes smaller as the folding is approached, so that the peak of the curve is not easily measurable. In particular, for a running belt, many disturbances are present and force the system to orbit in the neighborhood of the more attractive lower branch.

From the estimate values of v_T and $\tilde{\omega}_{1,v=0}$ it is possible to estimate the Young modulus of the belt material; however, the result is not close to the directly measured value. This is due

TABLE 1

Identified parameters in direct resonance condition

Eccentricity $\tilde{w}_0$ (m)	$\tilde{\omega}_{1,v=0}$ (rad/s)	v_T	δ_1
0·004	$2\pi 24.5$	6	0·026
0·0032	$2\pi 16.8$	6	0·023
0·0013	$2\pi 19{\cdot}4$	6	0·020
0·0006	$2\pi 19{\cdot}8$	8	0·016

to some simplifying assumptions on the boundary conditions (fixed ends), not completely in accord with the actual belt, where they are affected by the elasticity of the lower belt span. For this reason, it is preferable to identify v_T and create a dynamically equivalent model. The validity of this model will be proved in the next section.

3.2. PARAMETRIC RESONANCE

Increasing the axial speed, and therefore the excitation frequency, the resonance of the second mode is expected. Such frequency is approximately two times that of the first mode. In resonance conditions, the system should respond with the frequency of the excited second mode, and with its superharmonics and combinations. No quadratic non-linearities are present, so that the 1 : 2 internal resonance between the first and the second mode is not expected. In any case, the actual system responds with a one-half subharmonic, i.e., with half the excitation frequency and with a spatial shape close to that of the first mode. Such a response is due to the parametric excitation furnished by the axial tension fluctuation and was predicted by theoretical studies [9]. Here, one can note that the effect of the direct resonance on the second mode is suppressed by the presence of parametric instability; indeed, in the spectrum of measured time histories (which are not presented for the sake of brevity) we do not observe energy at the excitation frequency, but a subharmonic response occurs. In most of the operating conditions, the tension fluctuation does not play any role. Conversely, it can be experimentally observed that when the excitation frequency approaches twice that of a linear mode, this mode vibrates with very large amplitude and most of the energy transfers from high to low frequency.

In Figure 5(a), the response amplitude of the first mode in correspondence with the measurement point, versus the excitation frequency is shown for the case $\tilde{w}_0 = 0{\cdot}004$ m. The ratio $\Omega/2\omega_1$ means that the excitation frequency is normalized with respect to the first linear natural frequency ω_1 at the velocity $\bar{v}$ such that $\Omega(\bar{v})/\omega_1(\bar{v}) = 2$, which corresponds to the following dimensional frequency: $\tilde{\omega}_1 = 2\pi 17{\cdot}2$ rad/s; balls represent measured amplitudes, continuous lines represent the analytical curves. These are obtained by following the procedure outlined in section 2.3, equations 21(a, b), using the same damping ratio δ_1 and non-linear parameter v_T evaluated in primary resonance. The amplitude of the parameter p_1 is estimated by measuring the frequency variation at $v = 0$ and is equal to 0·4.

A second series of tests is performed for the cases $\tilde{w}_0 = 0{\cdot}0032, 0{\cdot}0013$ and $0{\cdot}0006$ m, using the values of parameters identified in direct resonance. The value of v_T identified in the case $\tilde{w}_0 = 0{\cdot}0006$ m has not been considered because it is very polluted. The tension fluctuation assumes the following values: $p_1 = 0{\cdot}35, 0{\cdot}2$ and $0{\cdot}1$ respectively for $\tilde{w}_0 = 0{\cdot}0032, 0{\cdot}0013$ and $0{\cdot}0006$ m. Comparisons between analytical response and measured amplitudes are shown in Figures 5(b–d).

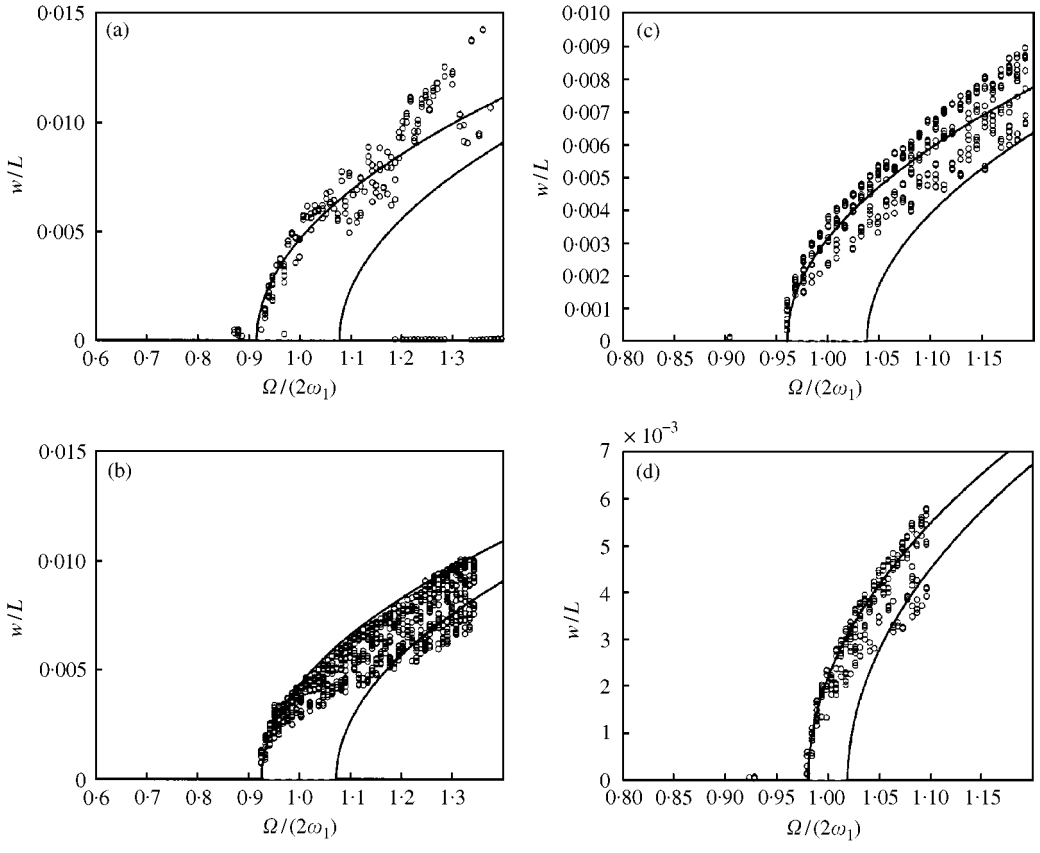

Figure 5. Amplitude frequency response curves. Parametric resonance, eccentricity: (a) 0·004 m; (b) 0·0032 m; (c) 0·0013 m; (d) 0·0006 m; (◦) measured amplitude; (—) analytical solutions.

The parameters p_1 and δ_1 establish the existence of parametric instability. In particular, parametric instability exists when p_1 is large with respect to δ_1, as can be found by means of the theoretical model. The parameter v_T gives the curvature of the bifurcated branches and p_1 gives the distance between them. It must be noted that the first branch, which is stable, fits very well the experimental data. The comparison confirms that: (1) the parameter identification in primary resonance is satisfactory; (2) the analytical model is able to predict the actual dynamics in different conditions. Coexisting periodic solutions are found when the excitation frequency is larger than 38 Hz [$\tilde{w}_0 = 0{\cdot}004$ m, Figure 5(a)], i.e., the system can respond both with a one half subharmonic and with a simple harmonic oscillation having very small amplitude. The upper branch indicates a subharmonic response with large amplitude.

Note that the upper branch does not present a maximum, i.e., increase the excitation frequency, the amplitude of oscillation increases monotonically up to a catastrophic level. Such a phenomenon is typical of the parametric resonance and is quite dangerous for actual systems. The lower branch of the curve can be obtained experimentally by constraining the system to orbit in the neighborhood of the lower level response (Figure 5a). In the present test, a mechanical constraint is introduced in the mid-span of the belt. After removing the constraint, the system does not jump to the upper branch and the fundamental frequency of vibration is equal to the excitation frequency. However, under a small perturbation, the dynamical system tends to return to the subharmonic orbit. This means that the

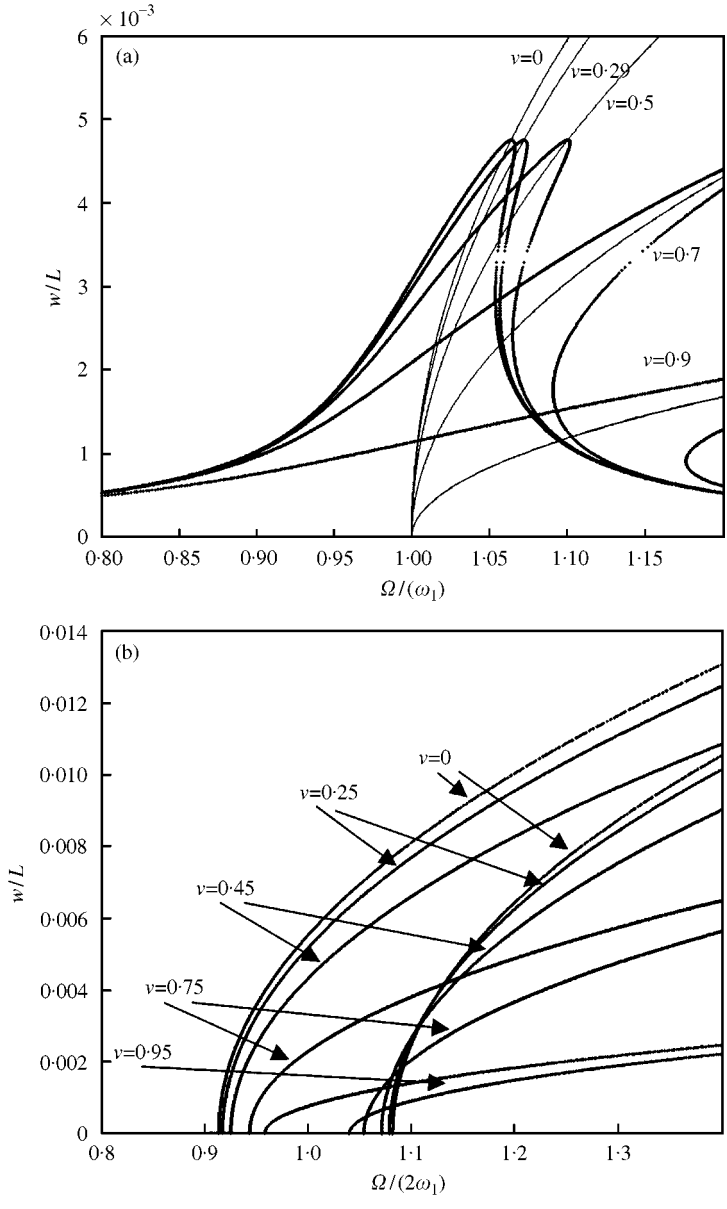

Figure 6. Effect of the axial speed, eccentricity 0·0032 m: (a) direct resonance, (b) parametric resonance.

subharmonic orbit is much more attractive than the harmonic orbit, giving further confirmation of the danger of the parametric resonance.

Even though the effect of axial velocity on the non-linear behavior has been analyzed in the past [3], it is of interest to quantify it in the light of the present results, namely, direct and parametric resonance. Let us suppose that the external excitation is not dependent upon the axial speed; in this case, resonances can be met for any axial speed. In Figure 6a, response frequency curves are depicted for axial speeds equal to 0, 29%v_{cr}, 50%v_{cr}, 75%v_{cr}, and 95%v_{cr}. As expected, the influence of the centrifugal forces, which reduce the natural frequencies, is a magnification of the non-linear character of the belt. In Figure 6(b) response frequency curves are depicted for axial speeds equal to 0, 25%v_{cr}, 45%v_{cr}, 75%v_{cr},

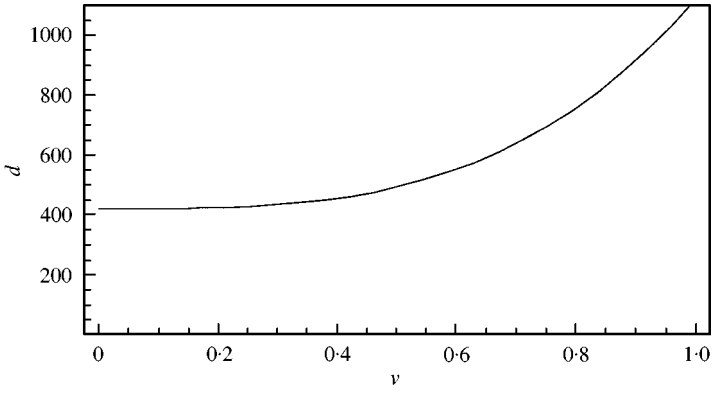

Figure 7. Nonlinear Normal Form coefficient d versus v, for $v_T = 6$.

and $95\%v_{cr}$. As in the previous case, the non-linearity notably grows; moreover, the two branches of the parametric response become closer to each other as the axial speed increases. Values of the axial speed equal to $29\%v_{cr}$ and $45\%v_{cr}$, correspond to the experimental cases carried out for the direct and parametric resonances respectively. This means that the region of instability of the trivial position decreases as the axial speed increases. Finally, in Figure 7, the behavior of the fundamental non-linear parameter d (see the normal form (13) where $A_2 = \mathrm{j}d$) is shown; its strong increase as v approaches v_{cr} explains Figures 6(a, b).

4. CONCLUSIONS

Direct and parametric resonances of a power transmission belt due to the presence of an eccentricity of one pulley are studied. Experimental observations with quantitative measurements are obtained by means of a triangulation laser telemeter and frequency response curves are drawn when the beam is harmonically excited close to the first and second linear natural frequencies. The asymptotic solution, which justifies the experimental evidence, allows for the identification of the main parameters of the equation of motion. A simple analytical model is obtained by one complex mode approximation. Good agreement between theoretical and experimental data, observed in several operating conditions, confirms the consistency of the analytical model and the identification of the parameters. The presence of a very stable parametric response is observed, the phenomenon looks particularly dangerous; in fact an extremely attractive subharmonic response is found, leading the system to collapse when the axial speed is large enough. To our knowledge, quantitative comparisons between theoretical and experimental data, with non-linear parametric identification, regarding axially moving systems, are not present in the existent literature.

REFERENCES

1. H. ASHLEY and G. HAVILAND 1950 *Journal of Applied Mechanics* **17**, 229–232. Bending vibrations of a pipe line containing flowing fluid.
2. R. D. SWOPE and W. F. AMES 1963 *Journal of Franklin Institute* **275**, 36–55. Vibrations of a moving threadline.

3. C. D. MOTE JR 1996 *Journal of Applied Mechanics* **33**, 463–464. On the non-linear oscillation of an axially moving string.
4. A. L. THURMAN and C. D. MOTE JR 1969 *Journal of Applied Mechanics* **36**, 83–91. Free, periodic, nonlinear oscillation of an axially moving strip.
5. J. A. WICKERT and C. D. MOTE JR 1990 *Journal of Applied Mechanics* **57**, 738–744. Classical vibration analysis of axially moving continua.
6. J. A. WICKERT 1992 *International Journal of Non-Linear Mechanics* **27**, 503–517. Non-linear vibration of a travelling tensioned beam.
7. F. PELLICANO and F. VESTRONI 2000 *Journal of Vibration and Acoustics* **122**, 21–30. Nonlinear dynamics and bifurcations of an axially moving beams.
8. A. G. ULSOY, J. E. WHITESELL and M. D. HOOVEN 1985 *Journal of Vibration, Acoustics, Stress, and Reliability in Design* **107**, 282–290. Design of Belt–Tensioner systems for dynamic stability.
9. E. M. MOCKENSTURM, N. C. PERKINS and G. A. ULSOY 1996 *Journal of Vibration and Acoustics* **118**, 346–351. Stability and limit cycles of parametrically excited, axially moving string.
10. S.-J. HWANG, N. C. PERKINS, A. G. ULSOY and R. J. MECKSTROTH 1994 *Journal of Vibration and Acoustics* **116**, 71–78. Rotational response and slip predictions of serpentine belt drive systems.
11. J. MOON and J. A. WICKERT 1997 *Journal of Sound and Vibration* **200**(4), 419–431. Non-linear vibration of power transmission belts.
12. F. PELLICANO, A. FREGOLENT and A. BERTUZZI 1998 *Proceedings of ISMA*23, *Leuven, Belgium*, Vol. III, 1531–1536. An experimental study on the transverse vibration of a power transmission belt.
13. A. A. N. AL-JAWI, C. PIERRE and A. G. ULSOY 1995 *Journal of Sound and Vibration* **179**, 243–266. Vibration localization in dual-span axially moving beams. Part I: formulation and results.
14. A. A. N. AL-JAWI, C. PIERRE and A. G. ULSOY 1995 *Journal of Sound and Vibration* **179**, 267–287. Vibration localization in dual-span axially moving beams. Part II: perturbation analysis.
15. A. A. N. AL-JAWI, A. G. ULSOY and C. PIERRE 1995 *Journal of Sound and Vibration* **179**, 289–312. Vibration localization in band-wheel systems: theory and experiment.
16. S.-J. HWANG and N. C. PERKINS 1992 *Journal of Sound and Vibration* **154**, 381–396. Supercritical stability of an axially moving beam. Part I: model and equilibrium analysis.
17. S.-J. HWANG and N. C. PERKINS 1992 *Journal of Sound and Vibration* **154**, 397–409. Supercritical stability of an axially moving beam. Part II: vibration and stability analyses.
18. H. POINCARE 1892 *Les Methodes Nouvelles de la Mechanique Celeste*. Paris: Gauthier-Villars.
19. A. D. BRYUNO 1989 *Local Methods in Nonlinear Differential Equations. Part I. The local Method of Nonlinear Analysis of Differential Equations. Part II. The Sets of Analyticity of a Normalizing Transformations*. New York, Heidelberg, Berlin: Springer Verlag.
20. A. H. NAYFEH 1993 *Method of Normal Forms*. New York: Wiley.
21. S. WIGGINS 1990 *Introduction to Applied Nonlinear Dynamical Systems and Chaos*. New York: Springer Verlag.
22. F. PELLICANO, M. AMABILI and A. F. VAKAKIS 2000 *Journal of Vibration and Acoustics* **122**, 355–364. Nonlinear vibrations and multiple resonances of fluid-filled, circular cylindrical shells. Part II: perturbation analysis.

APPENDIX A

Equation (9) can be specialized for $n = 1$, obtaining the following relationships:

$$M_1 = \pi^2(1 - v^2),$$

$$\mathbf{F}[(\xi_n(t)\boldsymbol{\phi}_n(x) + \xi_n^*(t)\boldsymbol{\phi}_n^*(x)), t]$$

$$= 2v\dot{w}_0(t) - \ddot{w}_0(t)\times(1 - x) - \frac{\mathrm{j}\exp[-\mathrm{j}\pi v(2 + x)]}{4}[\xi_1^* + \xi_1\exp(2\mathrm{j}\pi v x)]\pi^3 v^3$$

$$\times[\xi_1^{*2}(\exp\{2\mathrm{j}\pi v\} - 1) + \xi_1^2\exp\{2\mathrm{j}\pi v\}(\exp\{2\mathrm{j}\pi v\} - 1) - 4\mathrm{j}\pi v\xi_1\xi_1^*\exp\{2\mathrm{j}\pi v\}]v_T^2.$$

Coefficients of Equation (11) are

$$A_1 = -\frac{\pi^2(1 + v^2)v_T^2\sin(\pi v)(-\mathrm{j}\cos(\pi v) + \sin(\pi v))}{8v},$$

$$A_2 = \frac{\mathrm{j}\pi v_T^2(1 + 4\pi^2 v^2 + 8\pi^2 v^4 + 4\pi^2 v^6 - \cos(2\pi v))}{16v^2},$$

$$A_3 = -\frac{3\pi^2(1 + v^2)v_T^2(-1 + \cos(2\pi v) - \mathrm{j}\sin(2\pi v))}{16v},$$

$$A_4 = \frac{\pi v_T^2 \sin(\pi v)^2(\mathrm{j}\cos(2\pi v) + \sin(2\pi v))}{8v^2},$$

$$A_5 = \frac{2v\cos(\pi v) - \mathrm{j}(-\pi + 2\mathrm{j}\,v + \pi v^2 + 2v\sin(\pi v))}{\pi^3(-1 + v^2)^2},$$

$$A_6 = \frac{2v(\mathrm{j} + \mathrm{j}\cos(\pi v) + \sin(\pi v))}{\pi^2(-1 + v^2)},$$

$$c_1 = -\frac{\mathrm{j}\pi(1 + v^2)}{2},$$

$$c_2 = -\frac{(1 - \cos(2\pi v) + \mathrm{j}\sin(2\pi v))}{4v}.$$